Atmospheric
Chemistry
and Physics

Increased importance of aerosol–cloud interactions for surface PM$_{2.5}$ pollution relative to aerosol–radiation interactions in China with the anthropogenic emission reductions

Da Gao[1,2], **Bin Zhao**[1,2], **Shuxiao Wang**[1,2], **Yuan Wang**[3], **Brian Gaudet**[4], **Yun Zhu**[5], **Xiaochun Wang**[1,2], **Jiewen Shen**[1,2], **Shengyue Li**[1,2], **Yicong He**[1,2], **Dejia Yin**[1,2], and **Zhaoxin Dong**[1,2]

[1]State Key Joint Laboratory of Environment Simulation and Pollution Control, School of Environment, Tsinghua University, Beijing, 100084, China
[2]State Environmental Protection Key Laboratory of Sources and Control of Air Pollution Complex, Beijing, 100084, China
[3]Department of Earth System Science, Stanford University, Stanford, CA, USA
[4]Pacific Northwest National Laboratory, Richland, Washington, USA
[5]Guangdong Provincial Key Laboratory of Atmospheric Environment and Pollution Control, College of Environment and Energy, South China University of Technology, Guangzhou Higher Education Mega Center, Guangzhou, 510006, China

Correspondence: Bin Zhao (bzhao@mail.tsinghua.edu.cn)

Abstract. Surface fine particulate matter (PM$_{2.5}$) pollution can be enhanced by feedback processes induced by aerosol–radiation interactions (ARIs) and aerosol–cloud interactions (ACIs). Many previous studies have reported enhanced PM$_{2.5}$ concentrations induced by ARIs and ACIs for episodic events in China. However, few studies have examined the changes in the ARI- and ACI-induced PM$_{2.5}$ enhancements over a long period, though the anthropogenic emissions have changed substantially in the last decade. In this study, we quantify the ARI- and ACI-induced PM$_{2.5}$ changes for 2013–2021 under different meteorology and emission scenarios using the Weather Research and Forecasting model with Chemistry (WRF-Chem), and we investigate the driving factors behind the changes. Our results show that, in January 2013, when China suffered from the worst PM$_{2.5}$ pollution, the PM$_{2.5}$ enhancement induced by ARIs in eastern China (5.59 µg m^{-3}) was larger than that induced by ACIs (3.96 µg m^{-3}). However, the ACI-induced PM$_{2.5}$ enhancement showed a significantly smaller decrease ratio (51 %) than the ARI-induced enhancement (75 %) for 2013–2021, making ACIs more important for enhancing PM$_{2.5}$ concentrations in January 2021. Our analyses suggest that the anthropogenic emission reductions played a key role in this shift. Owing to only anthropogenic emission reductions, the ACI-induced PM$_{2.5}$ enhancement decreased by 43 % in January, which was lower than the decrease ratio of the ARI-induced enhancement (57 %). The relative change in ARI- and ACI-induced PM$_{2.5}$ enhancement in July was similar to the pattern observed in January, caused by anthropogenic emission reductions. The primary reason for this phenomenon is that the decrease in ambient PM$_{2.5}$ for 2013–2021 caused a disproportionately small decrease in the liquid water path (LWP) and an increase in the cloud effective radius (Re) under the condition of high PM$_{2.5}$ concentrations. Therefore, the surface solar radiation attenuation (and, hence, the boundary layer height reduction) caused by ACIs decreased slower than that caused by ARIs. Moreover, the lower decrease ratio of the ACI-induced PM$_{2.5}$ enhancement was dominated by the lower decrease ratio of ACI-induced secondary PM$_{2.5}$ component enhancement, which was additionally caused by the smaller decrease ratio of the air temperature reduction and the relative humidity (RH) increase. Our findings indicate that, with the decrease in ambient PM$_{2.5}$,

the ACI-induced PM$_{2.5}$ enhancement inevitably becomes more important. This needs to be considered in the formulation of control policies to meet the national PM$_{2.5}$ air quality standard.

1 Introduction

Aerosol–radiation interactions (ARIs) and aerosol–cloud interactions (ACIs) are important ways for aerosols to influence the climate (Rosenfeld et al., 2014; Seinfeld et al., 2016; Liu et al., 2018; Bellouin et al., 2020; Forster et al., 2021). The ARI represents the direct scattering and absorption of solar and infrared radiation by atmospheric aerosols; the ACI denotes the modification effects of atmospheric aerosols on the lifetime and the physical and optical properties of clouds.

Previous studies have documented that both ARIs and ACIs make important contributions to inhibiting the planetary boundary layer height (PBLH), cooling the near-surface air temperature, and increasing the relative humidity (RH) (Wang et al., 2014; Ding et al., 2016; Liu et al., 2018). Moreover, ACIs make contributions to changing precipitation and cloud chemistry (Zhao et al., 2017; Zhang et al., 2018). These feedbacks and changes are mostly conducive to increasing the haze severity (Wang et al., 2015; Zhang et al., 2018; Liu et al., 2018; Zhou et al., 2019; Zhang et al., 2020; Xiong et al., 2022; Lin, 2022). So far, numerous studies have evaluated the fine particulate matter (PM$_{2.5}$) enhancements caused by the decreases in downward shortwave radiation at the surface (SWDOWN), the PBLH, near-surface air temperature, precipitation, and increases in RH, especially during severe PM$_{2.5}$ pollution in China (Le et al., 2020). B. Zhang et al. (2015) and X. Zhang et al. (2018) quantified that the ARIs caused the PM$_{2.5}$ increases of 8.3 μg m^{-3} in 2013 and 4.0 μg m^{-3} in 2014. However, both positive and negative contributions of ACIs to PM$_{2.5}$ have been revealed (Forkel et al., 2012, 2015; Kong et al., 2015; B. Zhang et al., 2015; X. Zhang et al., 2018). Zhao et al. (2017) pointed out that the negative contribution of ACIs shown in some studies (Gustafson et al., 2007; Gong et al., 2015) is due to the relatively high prescribed values of cloud droplet number concentration (CDNC) or cloud condensation nuclei (CCN), which could not represent a rather clean condition. Besides, there might be a discrepancy between the enhancements induced by ARIs and ACIs for primary and secondary PM$_{2.5}$ components. The primary PM$_{2.5}$ components are mainly influenced by physical transport, while the secondary PM$_{2.5}$ components are also affected by chemical formation and decomposition. The lower air temperature and higher RH can help to condense gas precursors into secondary aerosol particles (Donahue et al., 2012) and to strengthen aqueous and heterogeneous reactions (Liu et al., 2018). On the contrary, Wu et al. (2020) pointed out that the ARIs may also suppress the formation of secondary aerosol because the atmospheric oxidizing capacity and photolysis rate can be changed dur-

ing the scattering and absorption of solar radiation. Therefore, not all changes in terms of meteorological factors are conducive to the increase of secondary PM$_{2.5}$, and these positive and negative contributions would influence the variations in primary and secondary PM$_{2.5}$ components. In a word, although the ARI and ACI processes mostly lead to a net PM$_{2.5}$ increase, the relative increasing rates of different aerosol components are fairly complex due to various physical and chemical processes.

In recent years, the Chinese government has successively proclaimed the policies of the Air Pollution Prevention And Control Action Plan and the Three-Year Action Plan To Win The Blue Sky Defense War, including the promotion of ultralow emission technologies in industrial sectors, the implementation of traffic restriction policies, and the transition from coal to gas in residential cooking. As a result, the annually averaged PM$_{2.5}$ concentrations in the Beijing–Tianjin–Hebei region, the Yangtze River Delta (YRD), and the Pearl River Delta have been reduced by 39.6 %, 34.2 %, and 27.7 % from 2013 to 2017, respectively (Wang et al., 2017; Ding et al., 2019). Meanwhile, sulfate and organic components have respectively decreased by 76 % and 70 % in the North China Plain (NCP) (Wang et al., 2019). Considering the sharp anthropogenic emission reduction and PM$_{2.5}$ concentration decrease, Moch et al. (2022) found that the decrease in mean PM$_{2.5}$ concentration from the winter months of 2012–2013 to the winter months of 2016–2017 in China weakened the cloud–snowfall–albedo feedback induced by the aerosol semi-direct effect. For air quality, Zhang et al. (2022) found that the decrease in black carbon from 2013 to 2017 in China reduced the enhanced PM$_{2.5}$ concentration induced by the ARIs by 1.8 μg m^{-3} in January and 0.3 μg m^{-3} in July.

However, none of the previous studies have systematically evaluated the changes in enhanced PM$_{2.5}$ concentrations in relation ARIs and ACIs in China over a long-term scale. Besides, the driving force and physical mechanisms for the changes are also yet to be explored. In this study, we try to investigate the enhanced PM$_{2.5}$ concentrations induced by ARIs and ACIs in 2013 over China and the impact of the changes to the meteorological background and anthropogenic emissions from 2013 to 2021 on ARI- and ACI-induced PM$_{2.5}$ enhancements and its components. Furthermore, the causes of PM$_{2.5}$ enhancement changes are analyzed.

2 Model and experimental design

2.1 Model configuration

The Weather Research and Forecasting model with Chemistry (WRF-Chem) version 4.2 has been used in this study. The model domain covers the whole land area of China with a horizontal resolution of $27\,\text{km} \times 27\,\text{km}$. There are 24 vertical layers from the surface to $50\,\text{hPa}$, with denser layers in the planetary boundary layer (PBL). Major physical options used in the model include the Morrison double-moment scheme (Morrison et al., 2009), the rapid radiative transfer model for GCMs (RRTMG) shortwave and longwave radiative transfer schemes (Iacono et al., 2008), the Eta similarity surface layer scheme (Janjic et al., 1994), the Noah land surface model with multiple parameterization options (Niu et al., 2011), the Bougeault and Lacarrere PBL scheme (Bougeault et al., 1989), and the Grell–Freitas ensemble cumulus scheme (Grell et al., 2014). For chemistry, we employ the SAPRC-99 (Statewide Air Pollution Research Center mechanism, version 1999) as the gas-phase chemistry mechanism (Carter, 2000). The aerosol module used in the study is the Model for Simulating Aerosol Interactions and Chemistry (MOSAIC) (Zaveri et al., 2008), which includes all major aerosol processes and represents the aerosol size distribution with eight size bins. The MOSAIC also incorporates the one-dimensional volatility basis set (VBS) framework that improves the simulation of secondary organic aerosol (Shrivastava et al., 2011). Rates for photolytic reactions are calculated using the Fast-J photolysis rate scheme (Wild et al., 2000). Additionally, we noted the poor ability of nitrate simulation in the WRF-Chem model. We improved the nitrate simulation by addressing the HONO underestimation in the model (Wang et al., 2015; Xue et al., 2020). More detailed information can be found in Sect. S1 in the Supplement. The meteorological initial and boundary conditions are derived from the National Centers for Environmental Prediction Final Analysis reanalysis data with resolutions of $1.0° \times 1.0°$ and $6\,\text{h}$ (http://rda.ucar.edu/datasets/ds083.2/, last access: 9 March 2023). The chemical initial and boundary conditions are acquired from the simulation results of the National Center for Atmospheric Research's Community Atmosphere Model with Chemistry (CAM-Chem, before 2020, https://www.acom.ucar.edu/cam-chem/cam-chem.shtml, last access: 10 March 2023) and the Whole Atmosphere Community Climate Model (WACCM, after 2020, https://www.acom.ucar.edu/waccm/download.shtml, last access: 10 March 2023) with resolutions of $0.94° \times 1.25°$ and $6\,\text{h}$.

The anthropogenic emission data in China for 2013–2021 are obtained from the ABaCAS-EI (Air Benefit and Cost and Attainment Assessment System-Emission Inventory) developed by Tsinghua University (Li et al., 2023). Specific emissions of SO_2, NO_x (NO and NO_2), NH_3, $PM_{2.5}$, and VOCs (volatile organic compounds) in 2013 and 2021 are presented in Table S2. The emission data in other countries are obtained from the IIASA emission inventory for 2015 (Zheng et al., 2019; Gao et al., 2020). The biogenic emission is calculated online by the Model of Emissions of Gases and Aerosols from Nature (MEGAN) v2.04 (Guenther et al., 2006). The dust emission is calculated online by the Goddard Chemistry Aerosol Radiation and Transport (GOCART) model coupled with the MOSAIC aerosol schemes (Zhao et al., 2010, 2013).

To account for the physical processes of aerosol–radiation–cloud feedbacks on meteorological factors and $PM_{2.5}$, the four-dimensional data assimilation (FDDA) is not utilized in our simulations. Aerosol optical depth, single scattering albedo, and asymmetry factors are calculated based on the Lorenz–Mie theory as a function of wavelength and three-dimensional location (Fast et al., 2006). Then, the aerosol optical properties are transferred to the RRTMG radiation scheme to calculate the impact of aerosol on the radiation balance (Iacono et al., 2008). As for the ACIs, activated aerosols are calculated by the Abdul-Razzak and Ghan scheme (Abdul-Razzak and Ghan, 2002) and are then coupled with the Morrison two-moment cloud microphysics scheme (Morrison et al., 2009). The prognostic cloud water content calculated by the Morrison scheme is input into the RRTMG scheme for the radiative transfer calculation. It should be noted that the prognostic aerosol does not influence cumulus clouds and ice nucleation in the model. The prognostic aerosol can only be activated as CCN. It does not directly contribute to ice nucleation, which is only influenced by air temperature and supersaturation (Kanji et al., 2017). Furthermore, CCN would influence grid-scale clouds. However, limited by the horizontal resolution of $27\,\text{km} \times 27\,\text{km}$, cumulus clouds could not be resolved in this grid.

2.2 Experimental design

As described in the introduction, the purpose of this study is to quantify the contributions of ARIs and ACIs to $PM_{2.5}$ concentrations under different emission scenarios. The simulation periods are January and July 2013 and 2021, representing winter and summer, respectively.

As shown in Table 1, the enhanced $PM_{2.5}$ concentration induced by ARIs and ACIs could be obtained via comparing the simulation results with ARIs or ACIs turned on or off. By setting the aer_ra_feedback to 0 in the model, the ARIs could be turned off, which means that the interaction between aerosol and radiation is prevented. The ACIs could be turned off through prescribing a CDNC of $25\,\text{cm}^{-3}$ in the microphysical scheme, which represents the average level in the pristine air (Bennartz, 2007). For example, the 13M13E_B, 13M13E_NR, and 13M13E_NRC shown in Table 1 represent the cases with ARI and ACI effects, without ARI effect, and without ARI and ACI effects in 2013, respectively. The ARI-induced $PM_{2.5}$ enhancement could be acquired by comparing the results of 13M13E_B and 13M13E_NR; the ACI-

Table 1. Case definition under different meteorological backgrounds and anthropogenic emissions with ARIs or ACIs turned on or off.

Case	Meteorology	Emission	ARI	ACI
13M13E_B	Jan and Jul 2013	Jan and Jul 2013	on	on
13M13E _NR	Jan and Jul 2013	Jan and Jul 2013	off	on
13M13E _NRC	Jan and Jul 2013	Jan and Jul 2013	off	off
21M13E_B	Jan and Jul 2021	Jan and Jul 2013	on	on
21M13E_NR	Jan and Jul 2021	Jan and Jul 2013	off	on
21M13E_NRC	Jan and Jul 2021	Jan and Jul 2013	off	off
21M21E_B	Jan and Jul 2021	Jan and Jul 2021	on	on
21M21E_NR	Jan and Jul 2021	Jan and Jul 2021	off	on
21M21E_NRC	Jan and Jul 2021	Jan and Jul 2021	off	off

induced PM$_{2.5}$ enhancement could be obtained by comparing the results of 13M13E_NR and 13M13E_NRC.

In order to obtain the changes in the ARI- and ACI-induced PM$_{2.5}$ enhancements from 2013 to 2021 caused by the variation in meteorological background and by the reduction in anthropogenic emissions, the control experiments (21M13E; three experiments: with ARI and ACI turned on, with ARI turned off and ACI turned on, and with ARI and ACI turned off) are designed with the meteorological background in 2021 and the anthropogenic emission in 2013. In the following, the 13M13E, 21M13E, and 21M21E represent the cases with meteorological background and anthropogenic emissions in 2013, meteorological background in 2021 and anthropogenic emissions in 2013, and meteorological background and anthropogenic emissions in 2021, respectively. Taking the ARI, for example, the change in the ARI-induced PM$_{2.5}$ enhancement from the variation in the meteorological background is obtained by subtracting the ARI-induced PM$_{2.5}$ enhancement in the 13M13E from that in the 21M13E (Eq. 1); the change in the ARI-induced PM$_{2.5}$ enhancement from the reduction in anthropogenic emissions is obtained by subtracting the ARI-induced PM$_{2.5}$ enhancement in the 21M13E from that in the 21M21E (Eq. 2). The calculations for the ACI-induced PM$_{2.5}$ enhancement are similar, as shown in Eqs. (3) and (4):

$$\text{ARI}_{met} = (21\text{M13E\_B} - 21\text{M13E\_NR}) - (13\text{M13E\_B} - 13\text{M13E\_NR}), \tag{1}$$

$$\text{ARI}_{emi} = (21\text{M21E\_B} - 21\text{M21E\_NR}) - (21\text{M13E\_B} - 21\text{M13E\_NR}), \tag{2}$$

$$\text{ACI}_{met} = (21\text{M13E\_NR} - 21\text{M13E\_NR}C) - (13\text{M13E\_NR} - 13\text{M13E\_NRC}), \tag{3}$$

$$\text{ACI}_{emi} = (21\text{M21E\_NR} - 21\text{M21E\_NRC}) - (21\text{M13E}_{NR} - 21\text{M13E}_{NRC}), \tag{4}$$

where the ARI$_{met}$ (ACI$_{met}$) and ARI$_{emi}$ (ACI$_{emi}$) represent the changes in the enhanced PM$_{2.5}$ concentration induced by the ARI (ACI) from 2013 to 2021 caused by the variation in the meteorological background and the reduction in anthropogenic emissions, respectively.

2.3 Model evaluation

To determine the accuracy and reliability of simulation results, the 13M13E_B and 21M21E_B simulations (Table 1) are verified using the observations. The variables checked in the evaluation contain the concentration and components of surface PM$_{2.5}$ and the meteorological factors, including air temperature (T2) and water vapor mixing ratio (Q2) at 2 m, wind speed (WS10) and wind direction (WD10) at 10 m, and cloud fraction (CF) and liquid water path (LWP).

Simulated temperature, wind, and water vapor are compared with the observations from the National Climate Data Center (NCDC, http://www.ncdc.noaa.gov/, last access: 12 February 2023). The evaluation shows that the absolute errors for T2, WS10, and Q2 are, respectively, less than 1°, 1 m s^{-1}, and 0.1 g kg^{-1} (Table S3), and those for WD10 are near to or less than 10°. For the simulation utilizing the FDDA, the benchmarks of biases proposed by Emery et al. (2001) are 0.7°, 0.6 m s^{-1}, 1.0 g kg^{-1}, and 20° for the T2, WS10, Q2, and WD10, respectively. The biases of the T2 and WS10 in our simulations have exceeded the benchmarks, while they are still similar to or smaller than those in most previous WRF-Chem applications without FDDA over east Asia (Zhang et al., 2015; Zhao et al., 2017).

Simulated CF and LWP are compared with the data from the Moderate-resolution Imaging Spectroradiometer (MODIS) aboard the Terra satellite (http://ladsweb.nascom.nasa.gov/data/search.html, last access: 12 February 2023). Overall, the CF and LWP simulations are in good agreement with the observations (Figs. S1 and S2). The high values of observed CF and LWP primarily appear in the south of China in January 2013 and 2021, and the high value of CF also occurs in the NCP region. The high values of CF and LWP in the south of China could be reproduced in the simulation, while the CF in the NCP region is slightly underestimated, which could be due to the imperfect cloud parameterization scheme in the model or the uncertainties in the retrieval of MODIS datasets. In July 2013 and 2021, part of the high-value area of the observed LWP and the most high-value area of the observed CF appear in the southwest of China and the east coast of China, which also could be captured by the simulation. In addition, high LWP also appears in Gansu and Sichuan provinces in July 2013 and in the YRD and Sichuan–Chongqing in July 2021, which are both well reproduced. The distributions of low values of observed CF and LWP in January and July of 2013 and 2021 are also well simulated.

The simulation of surface PM$_{2.5}$ concentration is compared with the data from the China National Environmental Monitoring Center (https://quotsoft.net/air/, last access: 12 February 2023). The evaluation shows that both the regional average value and spatial distribution of the simulated PM$_{2.5}$ concentration are in good agreement with the obser-

vational data. As shown in Fig. S3, the biases of the regional average $PM_{2.5}$ concentration in January and July of 2013 and 2021 are below $5\,\mu g\,m^{-3}$ in eastern China. In this study, eastern China includes most of the Chinese provinces except Xinjiang, Xizang, Ningxia, Qinghai, Gansu, inner-Mongolia, and Heilongjiang provinces, which contain the most polluted regions in China. In addition, the distributions of high simulated $PM_{2.5}$ concentrations are also consistent with the observations, such as the NCP region, the YRD region, and the Sichuan–Chongqing area.

The simulated $PM_{2.5}$ components are also reasonable compared with the observation data. Given that the $PM_{2.5}$ component data in 2013 are very rare, we sourced three sets of data in January 2013 in Beijing (Matthias et al., 2017), Handan (Zhang et al., 2015), and Shanghai (Li et al., 2015). The results show that the simulated $PM_{2.5}$ components are reproduced well generally. Specifically, the simulated $PM_{2.5}$ components are larger than half of the observational $PM_{2.5}$ components and less than double the observational $PM_{2.5}$ components (Fig. S4). Observed $PM_{2.5}$ component data in 2021 are from a data-sharing platform for the NCP region and its surrounding areas (Wang et al., 2019). Figure S5 shows the ratios of observations to simulations of ammonium, sulfate, BC, and organic carbon (OC) in January and July 2021. The results exhibit that almost all the ratios of $PM_{2.5}$ components are located between 0.5 and 2.0, while some ratios of sulfate in January, some ratios of the OC in January, and most ratios of the BC in January and July are beyond this range. However, these discrepancies will not cause obvious uncertainties in this research. Specifically, considering the low hygroscopicity of BC, BC overestimations in January and July 2021 probably bring about low uncertainties in ACI-induced $PM_{2.5}$ enhancement. To test the impact of simulated BC overestimation in January 2021 on ARI-induced $PM_{2.5}$ enhancement, we utilize another set of particulate matter (PM) source profiles (Liu et al., 2018) and conduct the simulations for January 2021. The results indicate that the ratios of simulated BC concentration to observational BC concentration are within 2.0. The ARI-induced $PM_{2.5}$ enhancement is $1.33\,\mu g\,m^{-3}$, which shows a negligible difference from the result ($1.37\,\mu g\,m^{-3}$) obtained using the original PM source profiles (Fig. S6). In view of the results in January 2021, the BC overestimation in July 2021 also probably brings about low uncertainties in ARI-induced $PM_{2.5}$ enhancement. However, the reduction in the simulated BC concentration in January 2021 does not necessarily mean that this set of PM source profiles is better than the original PM source profiles because this might be an accidental result caused by other uncertainties. For example, the current model underestimates the wet deposition of BC due to neglecting the increase in BC hygroscopicity brought about by BC aging. If this process is considered in the model, simulated BC concentrations might be better reproduced using original PM source profiles. Therefore, in this study, we still use the original results for our analysis.

The model also underestimates the sulfate concentration and overestimates part of the OC concentration in January 2021. We think that neither of these discrepancies will cause significant uncertainties in ARI- and ACI-induced $PM_{2.5}$ enhancement. Specifically, the majority of aerosols are scattering aerosols, and the $PM_{2.5}$ concentration in January 2021 is reproduced well. Therefore, we think that the impact of the sulfate underestimation on the ARI-induced $PM_{2.5}$ enhancement would be largely offset by the overestimation of other scattering-aerosol components, such as OC. In addition, the OC overestimation should not bring about significant uncertainty in ACI-induced $PM_{2.5}$ enhancement either because of the relatively lower hygroscopicity of OC compared to secondary inorganic aerosol. The underestimation of sulfate simulations in January 2021 also minimally affects ACI-induced $PM_{2.5}$ enhancement because the sulfate underestimation mainly occurs in the North China Plain, where cloud cover is low. In contrast, in southern cities such as Mianyang City in Sichuang Province, where there is plenty of cloud cover, the sulfate simulation was $4.19\,\mu g\,m^{-3}$ in January 2021, which is very close to the observed value of $4.25\,\mu g\,m^{-3}$ (Lin et al., 2022).

In summary, the performances of the WRF-Chem model in terms of the simulations of air quality and meteorological factors over China are fairly good, and the differences between simulations and observations are reasonable and acceptable.

3 Results and discussion

3.1 The impacts of ARI and ACI feedbacks on the meteorological factors and $PM_{2.5}$ concentrations in 2013

We comprehensively discuss the effects of ARIs and ACIs on the regional meteorological factors and $PM_{2.5}$ concentrations in January and July 2013. Figure 1 shows the impacts of ARI and ACI feedbacks on the SWDOWN, PBLH, T2, RH, and $PM_{2.5}$ concentration in January and July 2013. For the ARI, the SWDOWN decreases by 18.37 and $7.71\,W\,m^{-2}$ in January and July 2013, respectively, in eastern China. Since the incoming solar radiation reaching the ground is reduced by PM, the T2 and PBLH in eastern China further decrease by 0.30 and 0.03° and 28.34 and 8.75 m in January and July 2013, respectively. Meanwhile, the RH increases by 0.46 % and 0.08 % due to the water vapor accumulation in the suppressed planetary boundary layer (Liu et al., 2018). Ultimately, the $PM_{2.5}$ concentration increases by 5.59 and $0.13\,\mu g\,m^{-3}$ in eastern China (Fig. 1d). For the ACIs, affected by the cloud modified by the aerosol, the SWDOWN, T2, and PBLH decrease by 7.54 and $14.03\,W\,m^{-2}$, 0.18 and 0.17°, and 10.89 and 24.31 m, and the RH increases by 0.34 % and 0.37 % in January and July 2013 in eastern China, respectively. As a result, the $PM_{2.5}$ concentration increases by 3.96 and $2.20\,\mu g\,m^{-3}$ in eastern China. Figure 2 shows

that the regionally averaged values and spatial distributions of $PM_{2.5}$ enhancements induced by ARIs and ACIs in 2013 are in line with the results of previous studies (Zhao et al., 2017; Zhang et al., 2018).

Overall, the enhanced $PM_{2.5}$ concentration induced by ARIs is greater than that induced by ACIs in January 2013, which is due to the relatively low LWP in the high-$PM_{2.5}$-concentration area. However, it shows the opposite situation in July 2013 owing to the plentiful cloud cover in warm July (Zhang et al., 2018).

3.2 The shift in the $PM_{2.5}$ enhancements induced by ARIs and ACIs

As discussed in Sect. 3.1, the enhanced $PM_{2.5}$ concentrations induced by ARIs and ACIs exhibit obvious spatial and seasonal variations in 2013. However, due to the variations in meteorological background and the reduction in anthropogenic emissions from 2013 to 2021, their joint and individual impacts on the ARI- and ACI-induced $PM_{2.5}$ enhancements are still unclear. Figure 2 shows the ARI- and ACI-induced $PM_{2.5}$ enhancements in the experiments of 13M13E, 21M13E, and 21M21E in January and July.

As shown in Fig. 2, from 2013 to 2021, the $PM_{2.5}$ concentration enhancement induced by the ARIs in January decreases by 75 % (from 5.59 to 1.37 $\mu g\, m^{-3}$). Zhang et al. (2022) also found that the ARI effect over China weakens during 2013–2017, and the ratio of $PM_{2.5}$ enhancement to the ambient $PM_{2.5}$ concentration decreases from 5.40 % to 3.30 %. The decline of the $PM_{2.5}$ enhancement ratio (2.10 %) is lower than that in this study (3.26 %) due to the continuous emission reductions after 2017. On the other hand, the ACI-induced $PM_{2.5}$ enhancement decreases by 51 %, from 3.96 to 1.93 $\mu g\, m^{-3}$. With lower percentage decreases in the $PM_{2.5}$ enhancement, the ACI-induced $PM_{2.5}$ enhancement exceeds the ARI-induced $PM_{2.5}$ enhancement in January 2021. In July, both the ARI- and ACI-induced $PM_{2.5}$ enhancements show decreasing trends; the percentage decreases of the ARI-induced (31 %) and ACI-induced (34 %) $PM_{2.5}$ enhancements are very close.

The contributions of the meteorological background variation and anthropogenic emission reductions to the changes in the ARI- and ACI-induced $PM_{2.5}$ enhancements are different. Due to the meteorological background changes from 2013 to 2021, the ARI- and ACI-induced $PM_{2.5}$ enhancements show different characteristics in January and July. It can be seen that the ARI-induced $PM_{2.5}$ enhancement decreases from 5.59 to 3.15 $\mu g\, m^{-3}$ with the variation in the meteorological background in January, while it increases from 0.13 to 0.27 $\mu g\, m^{-3}$ in July. The primary reason for the difference is that the ambient $PM_{2.5}$ concentration decreases in January but increases in July due to different meteorological backgrounds. The ACI-induced $PM_{2.5}$ enhancement changes slightly from 3.96 to 3.40 $\mu g\, m^{-3}$ in January due to the variation in the meteorological background. However, it

increases from 2.20 to 3.31 $\mu g\, m^{-3}$ in July because of a large aerosol-induced LWP increase in July 2021.

Considering the reduction in anthropogenic emissions, the ARI- and ACI-induced $PM_{2.5}$ enhancements both show declining trends (middle and right columns in Fig. 2). The ARI-induced $PM_{2.5}$ enhancement decreases by 56.51 % in January, from 3.15 to 1.37 $\mu g\, m^{-3}$. The ACI-induced $PM_{2.5}$ enhancement decreases by 43.24 %, from 3.40 to 1.93 $\mu g\, m^{-3}$. The percentage decrease in the ACI-induced $PM_{2.5}$ enhancement is lower than that of the ARI-induced in January, which also occurs in July, when the ARI-induced $PM_{2.5}$ enhancement decreases by 66.67 % (from 0.27 to 0.09 $\mu g\, m^{-3}$) and the ACI-induced $PM_{2.5}$ enhancement decreases by 56.50 % (from 3.31 to 1.44 $\mu g\, m^{-3}$).

In summary, both the variation in the meteorological background and the reduction in anthropogenic emissions play important roles in changing the ARI- and ACI-induced $PM_{2.5}$ enhancements. However, the decreases in ARI- and ACI-induced $PM_{2.5}$ enhancements from 2013 to 2021 are primarily attributed to the reduction in anthropogenic emissions. In addition, the percentage decrease in the ACI-induced $PM_{2.5}$ enhancements is lower than that induced by the ARIs in both January and July. Therefore, the ACI-induced $PM_{2.5}$ enhancement has become increasingly important in both January and July from 2013 to 2021.

3.3 The changes in the enhanced $PM_{2.5}$ components induced by the ARIs and the ACIs

In terms of the anthropogenic emission reductions, the percentage decrease in the ACI-induced $PM_{2.5}$ enhancement is lower than that induced by the ARIs in both January and July. We find that the difference is primarily from the different percentage decreases in the secondary $PM_{2.5}$ component enhancements induced by ARIs and ACIs.

Figure 3 shows the percentage decreases in ARI- and ACI-induced $PM_{2.5}$ component enhancements caused by the anthropogenic emission reductions in January and July. It can be seen that the differences between the percentage decreases in the ARI- and ACI-induced enhancements of sulfate, nitrate, ammonium, and OC are larger than those of BC and other inorganic aerosol (OIN). OIN refers to inorganic compositions other than sulfate, nitrate, ammonium, and BC. These compositions include sea salt and mineral elements. Specifically, the differences between the percentage decreases for sulfate, nitrate, ammonium, and OC enhancements are 34.66 %, 40.20 %, 13.80 %, and 25.65 % respectively, and the values for OIN and BC are 8.67 % and 6.67 %. This result indicates that the lower decrease in the ACI-induced $PM_{2.5}$ concentration enhancement is mainly due to the small decrease in the ACI-induced enhancements of secondary $PM_{2.5}$ components. The main causes will be illustrated in Sect. 3.4.
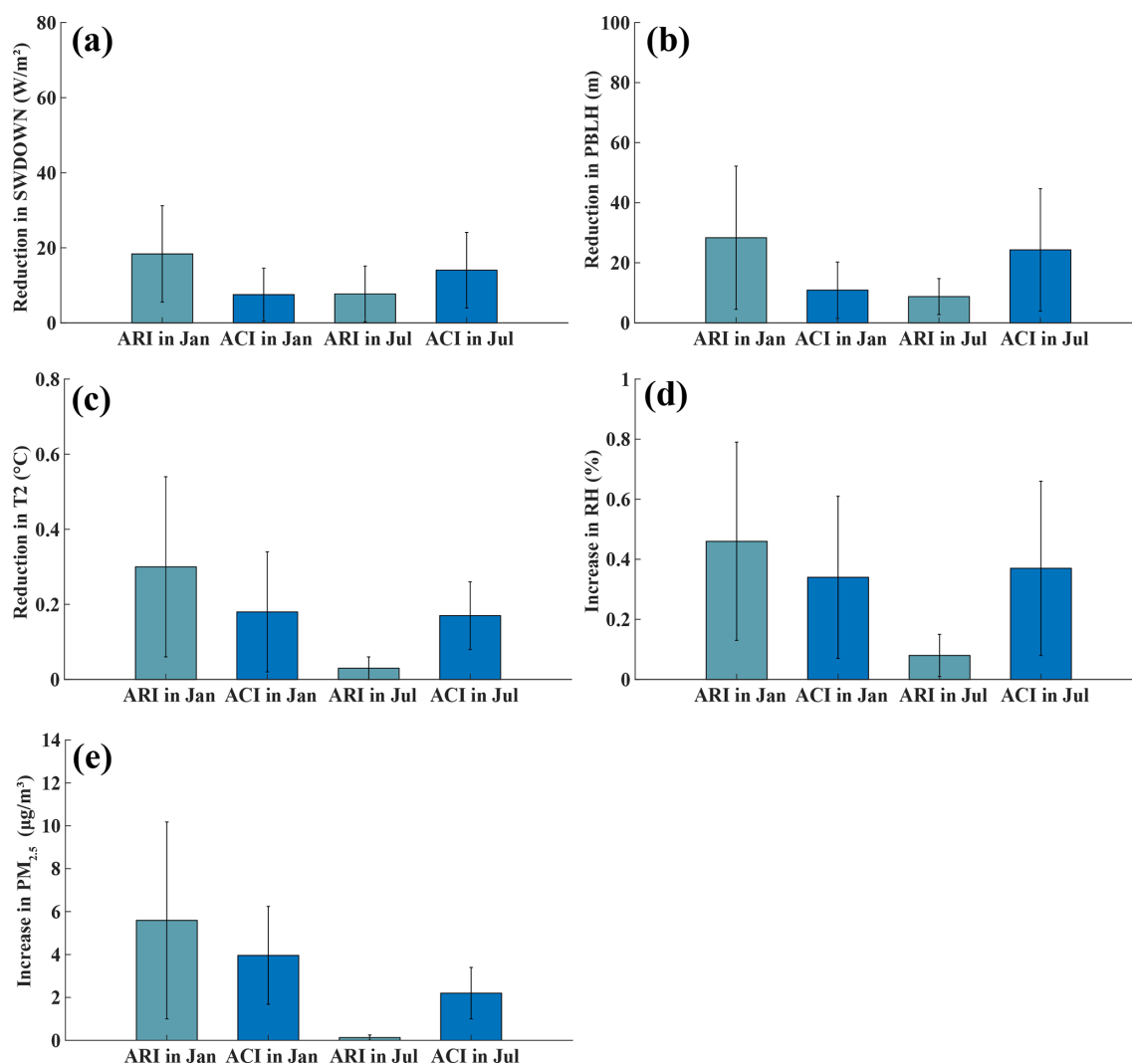
Figure 1. The regionally averaged reductions of **(a)** downward shortwave radiation at the surface (SWDOWN), **(b)** planetary boundary layer height (PBLH), **(c)** 2 m air temperature (T2), and increments of **(d)** relative humidity (RH) and **(e)** fine particulate matter ($PM_{2.5}$) concentration induced by the aerosol–radiative interaction (ARI) and aerosol–cloud interaction (ACI) in January and July 2013 in eastern China. The error bars represent the standard deviations for different meteorological factors and $PM_{2.5}$ concentrations induced by ARIs and ACIs in January and July 2013 in eastern China.

3.4 Causes for the increased importance of ACIs

3.4.1 Explanation from the perspective of meteorological changes

As discussed in previous studies, the decrease in PBLH and T2 and the increase in RH are tightly related to the ARI- and ACI-induced $PM_{2.5}$ enhancements (Donahue et al., 2012; Ding et al., 2016; Moch et al., 2022; Liu et al., 2018). From the perspective of the ARI- and ACI-induced changes in meteorological factors, we investigate the primary reasons for the increasing importance of the ACI-induced $PM_{2.5}$ enhancement under the reduction of anthropogenic emissions.

Figure 4 shows the percentage decreases in ARI- and ACI-induced decreases of SWDOWN, PBLH, and T2 and the in-

creases in RH due to the reduction of anthropogenic emissions from 2013 to 2021. In January, in order to illustrate the reasons for the lower percentage decrease in the ACI-induced $PM_{2.5}$ enhancement clearly, we take the highly polluted NCP region as an example. As shown in Fig. 4c, the percentage decreases in the ACI-induced declines in SWDOWN (19 %), PBLH (27 %), and T2 (20 %) and the increase in RH (24 %) are lower than those of the ARI-induced declines in SWDOWN (29 %), PBLH (39 %), and T2 (32 %) and the increase in RH (36 %). The phenomenon in July is similar to that in January (Fig. 4a and b). To our knowledge, the PBLH and T2 are determined by the incoming solar radiation at the surface, and they can strongly influence the RH. So the lower percentage decrease in the ACI-induced reductions of PBLH
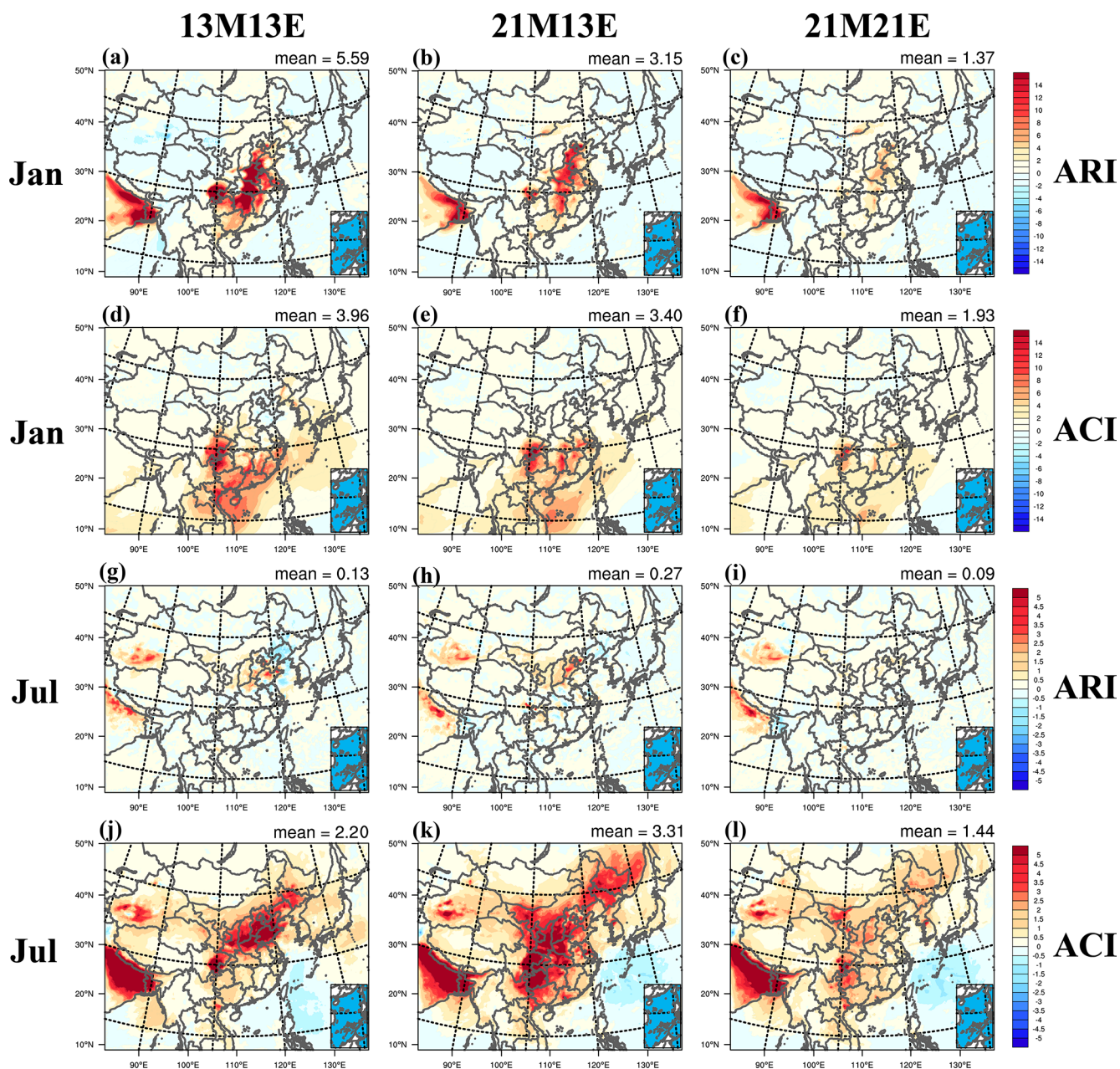
Figure 2. The distributions of enhanced $PM_{2.5}$ concentrations (unit: $\mu g\,m^{-3}$) induced by the ARIs (first and third rows) and the ACIs (second and fourth rows) in January (first and second rows) and July (third and fourth rows) in the experiments of 13M13E (left column), 21M13E (middle column), and 21M21E (right column).

and T2 and the increase in RH could be explained by the lower percentage decrease in the ACI-induced SWDOWN reduction.

We believe that the relatively lower decrease in the ACI-induced SWDOWN reduction is inevitable under high ambient $PM_{2.5}$ concentrations. As shown in Fig. S8b, the SWDOWN reduction induced by the ARI shows a linear relationship with the decline in ambient $PM_{2.5}$ concentration, which is similar to the findings of Zhou et al. (2018). In contrast, the decrease in the SWDOWN reduction induced by the ACI is lower than that induced by the ARI due to the ambient $PM_{2.5}$ decrease in the highly $PM_{2.5}$-polluted regime. The reason is that the decrease in ambient $PM_{2.5}$ concentration directly weakens the ARI-induced SWDOWN reduction, but it has only a minor impact on the ACI-induced SWDOWN reduction because the change in LWP and cloud effective radius (Re) induced by ACI is not sensitive to the $PM_{2.5}$ reduction in the $PM_{2.5}$-polluted regime. In our simulations, the
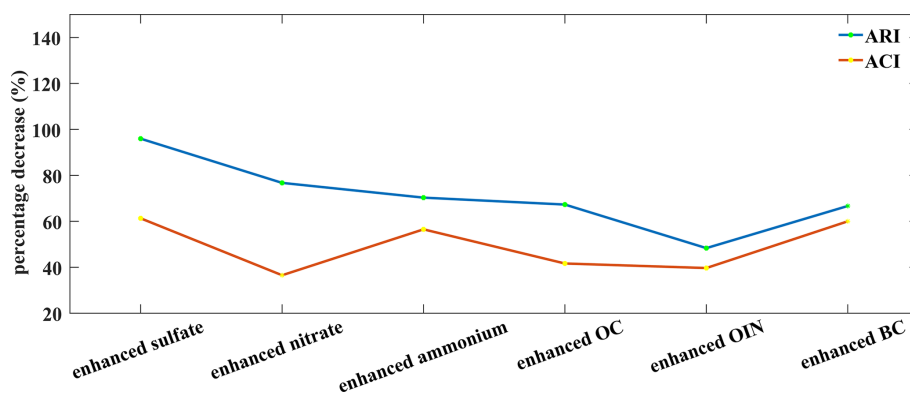
Figure 3. Percentage decreases (21M13E−21M21E)/21M13E) of the spatially and temporally averaged ARI- and ACI-induced $PM_{2.5}$ component enhancements in eastern China in January and July caused by the anthropogenic emission reductions from 2013 to 2021.

influence of the ACI-induced Re change is relatively smaller than that of the ACI-induced LWP change with a large decrease in $PM_{2.5}$ concentration (Fig. S7). Therefore, we are only concerned with the change in ACI-induced LWP with a reduction in $PM_{2.5}$. As shown in Fig. S8a, when the ambient $PM_{2.5}$ concentration exceeded $15\,\mu g\,m^{-3}$, the decrease in ACI-induced LWP increase was relatively low, with a $PM_{2.5}$ reduction from 120 to $15\,\mu g\,m^{-3}$, indicating that aerosols are not a key limiting factor to cloud formation in this range. Note that when the ambient $PM_{2.5}$ concentration decreases to $15\,\mu g\,m^{-3}$, the weakening of the SWDOWN reduction induced by the ACI might be larger than that induced by the ARI. This is because the decrease in the ACI-induced LWP increase is relatively fast, with a $PM_{2.5}$ reduction from 15 to $0\,\mu g\,m^{-3}$. Previous studies have demonstrated that the decrease in ACI-induced LWP increase is relatively fast or slow with the ambient $PM_{2.5}$ reduction in the $PM_{2.5}$-clean or $PM_{2.5}$-polluted conditions, respectively (Myhre et al., 2007; Savane et al., 2015). The regional and temporal average $PM_{2.5}$ concentration in eastern China in January and July, simulated using background meteorology in 2021 and emissions in 2013, is 63 and $25\,\mu g\,m^{-3}$, which is much higher than $15\,\mu g\,m^{-3}$. Therefore, the decrease in the ACI-induced SWDOWN reduction in both months is weak.

In particular, the lower PBLH caused by ARIs and ACIs will enhance the accumulation of all the $PM_{2.5}$ components, but the higher RH and lower T2 induced by the ARIs and ACIs could promote the production of extra secondary $PM_{2.5}$ components through strengthening aqueous and heterogeneous reactions, causing gas precursors to condense into particle matter (Donahue et al., 2012; Liu et al., 2018). Therefore, a lower percentage decrease in the T2 reduction and RH increase induced by the ACI is more likely to weaken the decrease in the enhancements of secondary $PM_{2.5}$ components. This explains well the lower percentage decreases in the enhancements of secondary $PM_{2.5}$ components induced by the ACIs compared to those induced by the ARIs, as shown in Fig. 3.

3.4.2 Explanation from the perspective of $PM_{2.5}$ concentration distribution changes

Ambient $PM_{2.5}$ concentration is the fundamental factor in triggering the ARI and the ACI. In order to further explore the reasons for the increasing importance of enhanced $PM_{2.5}$ concentrations induced by ACIs, we discuss the characteristics of enhanced $PM_{2.5}$ concentrations induced by ARIs and ACIs under different $PM_{2.5}$ pollution levels. Given that this study mainly focuses on the change in ARI- and ACI-induced $PM_{2.5}$ enhancement in the $PM_{2.5}$-polluted regime, we only discuss these changes within the $PM_{2.5}$ concentration range of 15–$180\,\mu g\,m^{-3}$.

The $PM_{2.5}$ concentration is divided into 11 levels from 15 to $180\,\mu g\,m^{-3}$. As shown in Fig. 5a, in the heavily $PM_{2.5}$-polluted regime (135–$180\,\mu g\,m^{-3}$), the decrease in SWDOWN induced by ARIs is much larger than that induced by ACIs (Fig. S9a). Then, the decrease in PBLH and T2 and the increase in RH induced by ARIs are also larger than those induced by ACIs (Fig. S9b–d). Thus, the enhanced $PM_{2.5}$ induced by the ARIs is much larger than that induced by the ACIs (Fig. 5a). However, when the $PM_{2.5}$ concentration decreases to the range of 15–$45\,\mu g\,m^{-3}$, the decreases in SWDOWN, PBLH, and T2 and the increase in RH induced by ACIs significantly exceed those induced by ARIs. Thus, the ACI-induced $PM_{2.5}$ enhancement significantly exceeds the ARI-induced $PM_{2.5}$ enhancement and becomes more important. This indicates the fast decrease in the ARI-induced $PM_{2.5}$ enhancement and the increasing contribution of the ACI-induced $PM_{2.5}$ enhancement with the decrease in the $PM_{2.5}$ concentration. In summary, the percentage decrease in the $PM_{2.5}$ enhancement induced by ACIs is weaker than that induced by ARIs with the decrease in $PM_{2.5}$ concentration because of the lower percentage decrease in the ACI-induced SWDOWN, which causes the lower percentage decrease in the ACI-induced PBLH and T2 reduction and the RH increase. Furthermore, as shown in Fig. S8a, the low percentage decrease in the ACI-induced SWDOWN reduc-
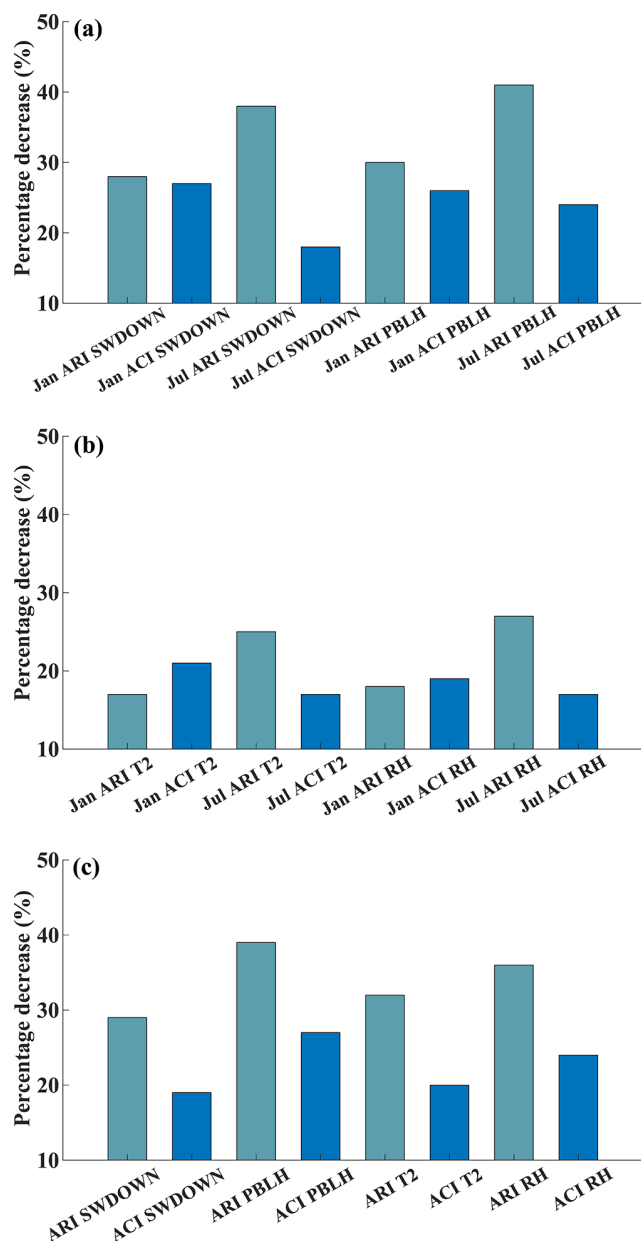
Figure 4. The percentage decreases in the regional averages of **(a)** the decrease in SWDOWN and PBLH and **(b)** the T2 reduction and RH increase induced by ARIs and ACIs in eastern China caused by the anthropogenic emission reductions in January and July from 2013 to 2021; **(c)** is the same as **(a)** and **(b)** but in the NCP region in January.

tion is due to a low decrease in the ACI-induced LWP in the $PM_{2.5}$-polluted regime. Considering the decrease in the ambient $PM_{2.5}$ concentration due to the anthropogenic emission reductions from 2013 to 2021 (Fig. 5b), the ACI-induced $PM_{2.5}$ enhancement certainly contributes more to the total $PM_{2.5}$ concentration in 2021.

4　Conclusions

Under the background of sharped anthropogenic emission reductions, this study investigates changes in the ARI- and ACI-induced $PM_{2.5}$ enhancements for 2013–2021 and explores the causes for these changes from the perspectives of meteorological factors and $PM_{2.5}$ concentration distributions.

The results show that the enhanced $PM_{2.5}$ induced by the ARI ($5.59\,\mu g\,m^{-3}$) is greater than that induced by the ACI ($3.96\,\mu g\,m^{-3}$) in January 2013. However, the ARI- and ACI-induced $PM_{2.5}$ enhancements decrease from 5.59 and $3.96\,\mu g\,m^{-3}$ to 1.37 and $1.93\,\mu g\,m^{-3}$ in January, and they decrease by 75 % and 51 % for 2013–2021. The smaller decrease ratio (51 %) for ACI-induced $PM_{2.5}$ enhancements implies that ACIs become more important for enhancing $PM_{2.5}$ concentrations in January 2021. Furthermore, we separated the contributions of meteorological background variations and anthropogenic emission reductions. Compared with the meteorological background variation, anthropogenic emission reductions play a more important role in causing the decrease in ARI- and ACI-induced $PM_{2.5}$ enhancements. Owing to only emission reductions, the enhanced $PM_{2.5}$ concentrations induced by the ARI and ACI decrease by 56 % and 43% in January and 66 % and 56 % in July, respectively. The ACI-induced $PM_{2.5}$ enhancement becomes increasingly important in both January and July for 2013–2021. More specifically, the lower percentage decrease in the ACI-induced $PM_{2.5}$ enhancement is dominated by the lower decrease in the enhancements of secondary $PM_{2.5}$ components.

The lower percentage decrease in the enhanced $PM_{2.5}$ induced by the ACIs is due to the lower percentage decrease in the ACI-induced SWDOWN reduction, which is because of the lower decrease in the LWP and the increase in the Re caused by the ambient $PM_{2.5}$ decrease in the highly $PM_{2.5}$-polluted regime (Fig. 6). At the same time, the lower percentage decreases in the T2 reduction and the RH increase induced by the ACIs further lead to the lower percentage decrease in the enhancements of the ACI-induced secondary $PM_{2.5}$ components (Fig. 6). Notably, due to relative lower percentage decrease in the ACI-induced SWDOWN reduction in the highly $PM_{2.5}$-polluted regime, the increasing importance of ACI-induced $PM_{2.5}$ enhancement is a matter of course with the ambient $PM_{2.5}$ decrease.

This study has important implication for the $PM_{2.5}$ control. As we know, ARI- and ACI-induced $PM_{2.5}$ enhancements make a non-negligible contribution to the deterioration of $PM_{2.5}$ air quality. Previous research has investigated the impact of anthropogenic emission reductions on the ARI-induced $PM_{2.5}$ enhancement (Zhou et al., 2019). But compared with $PM_{2.5}$ enhancement induced by ARIs, that induced by ACIs is more complicated and harder to be alleviated. Our findings have further revealed that the ACI-induced $PM_{2.5}$ enhancement is getting more important relative to that
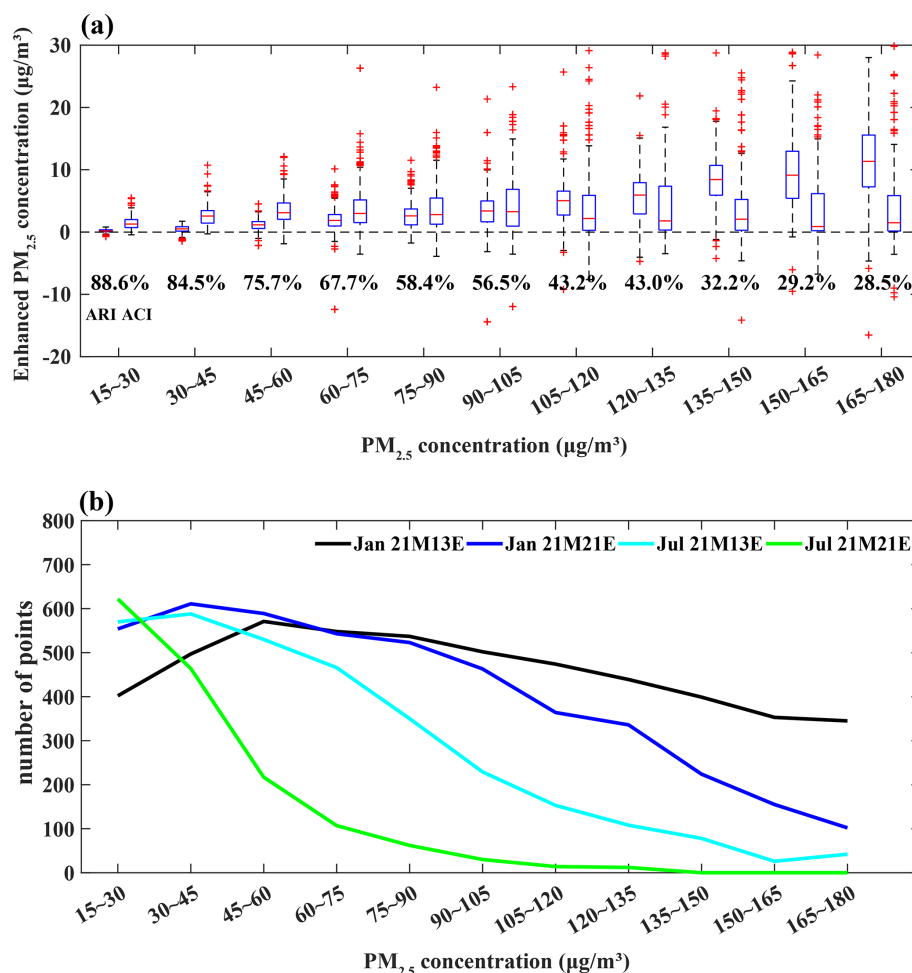
Figure 5. (a) The enhanced $PM_{2.5}$ concentrations induced by ARIs and ACIs at different ambient $PM_{2.5}$ levels. These data are from the simulations for January and July in the experiments of 21M13E and 21M21E. The percentage represents the ratio of the ACI-induced $PM_{2.5}$ enhancement to the sum of ARI- and ACI-induced $PM_{2.5}$ enhancements. (b) The distributions of ambient $PM_{2.5}$ levels in January and July in the experiments of 21M13E and 21M21E.

induced by ARIs. This is especially true in cloud-prone areas, like the Sichuan–Chongqing area, which have witnessed rather weak decreases in ACI-induced $PM_{2.5}$ concentrations in the past decade due to weak decreases in the aerosol-induced LWP under the condition of high ambient $PM_{2.5}$ level (Fig. 2). The ACI-induced $PM_{2.5}$ enhancement needs to be considered more seriously in the formulation of control polices to meet national $PM_{2.5}$ air quality standards, especially in cloud-prone areas with high ambient $PM_{2.5}$ concentrations. To control ACI-induced $PM_{2.5}$ enhancement, first, a larger emission reduction is necessary in cloudy areas compared to in less cloudy areas to bring about a noticeable decrease in ACI-induced LWP in response to $PM_{2.5}$ reduction. Second, secondary inorganic aerosol (SNA), which is an important component of total aerosol, has a large influence on the ACI-induced $PM_{2.5}$ enhancement because of its high hygroscopicity. This makes it easy for SNA to be activated as CCN and influence LWP. We think that it is crucial to make

substantial decreases in the precursors of SNA, such as SO_2, NO_x, and NH_3 species. These decreases could substantially decrease SNA. A large decrease in SNA would enhance the ACI-induced LWP response to $PM_{2.5}$ reduction and cause a large decrease in ACI-induced $PM_{2.5}$ enhancement. In addition, relative to ARI-induced $PM_{2.5}$ enhancement, the lower decrease in ACI-induced $PM_{2.5}$ enhancement is mainly because of the small decrease in ACI-induced enhancements of secondary $PM_{2.5}$ components. A substantial decrease in SNA would make the decrease ratio of ACI-induced $PM_{2.5}$ enhancement approach the more rapid decrease ratio of ARI-induced $PM_{2.5}$ enhancement.
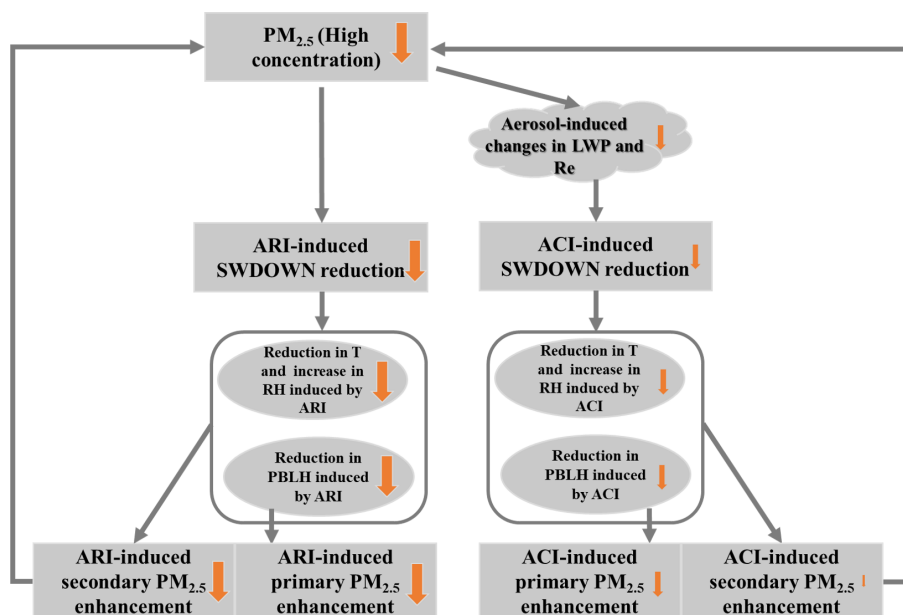
Figure 6. Schematic diagram for the decrease in ARI- and ACI-induced primary and secondary PM$_{2.5}$ enhancement due to the reduction in ambient PM$_{2.5}$ concentrations. The size of the arrows represents the magnitude of the changes due to the reduction in ambient PM$_{2.5}$ concentration.

References

Abdul-Razzak, H. and Ghan, S. J.: A parameterization of aerosol activation – 3. Sectional representation, J. Geophys. Res.-Atmos., 107, 4026, https://doi.org/10.1029/2001jd000483, 2002.

Bellouin, N., Quaas, J., Gryspeerdt, E., Kinne, S., Stier, P., Watson-Parris, D., Boucher, O., Carslaw, K. S., Christensen, M., Daniau, A. L., Dufresne, J. L., Feingold, G., Fiedler, S., Forster, P., Gettelman, A., Haywood, J. M., Lohmann, U., Malavelle, F., Mauritsen, T., McCoy, D. T., Myhre, G., Mulmenstadt, J., Neubauer, D., Possner, A., Rugenstein, M., Sato, Y., Schulz, M., Schwartz, S. E., Sourdeval, O., Storelvmo, T., Toll, V., Winker, D., and Stevens, B.: Bounding Global Aerosol Radiative Forcing of Climate Change, Rev. Geophys., 58, e2019RG000660, https://doi.org/10.1029/2019RG000660, 2020.

Bennartz, R.: Global assessment of marine boundary layer cloud droplet number concentration from satellite, J. Geophys. Res.-Atmos., 112, D02201, https://doi.org/10.1029/2006jd007547, 2007.

Bougeault, P. and Lacarrere, P.: Parameterization Of Orography-Induced Turbulence In a Mesobeta-Scale Model, Mon. Weather Rev., 117, 1872–1890, https://doi.org/10.1175/1520-0493(1989)117<1872:Pooiti>2.0.Co;2, 1989.

Carter, W. P. L.: Documentation of the SAPRC-99 Chemical Mechanism for VOC Reactivity Assessment, Contract No. 92-329 and 95-308, California Air Resources Board, 2000.

Ding, A. J., Huang, X., Nie, W., Sun, J. N., Kerminen, V. M., Petaja, T., Su, H., Cheng, Y. F., Yang, X. Q., Wang, M. H., Chi, X. G., Wang, J. P., Virkkula, A., Guo, W. D., Yuan, J., Wang, S. Y., Zhang, R. J., Wu, Y. F., Song, Y., Zhu, T., Zilitinkevich, S., Kulmala, M., and Fu, C. B.: Enhanced haze pollution by black carbon in megacities in China, Geophys. Res. Lett., 43, 2873–2879, https://doi.org/10.1002/2016GL067745, 2016.

Ding, D., Xing, J., Wang, S. X., Liu, K. Y., and Hao, J. M.: Estimated Contributions of Emissions Controls, Meteorological Factors, Population Growth, and Changes in Baseline Mortality to Reductions in Ambient $PM_{2.5}$ and $PM_{2.5}$-Related Mortality in China, 2013–2017, Environ. Health Persp., 127, 067009, https://doi.org/10.1289/Ehp4157, 2019.

Donahue, N. M., Henry, K. M., Mentel, T. F., Kiendler-Scharr, A., Spindler, C., Bohn, B., Brauers, T., Dorn, H. P., Fuchs, H., Tillmann, R., Wahner, A., Saathoff, H., Naumann, K. H., Mohler, O., Leisner, T., Muller, L., Reinnig, M. C., Hoffmann, T., Salo, K., Hallquist, M., Frosch, M., Bilde, M., Tritscher, T., Barmet, P., Praplan, A. P., DeCarlo, P. F., Dommen, J., Prevot, A. S. H., and Baltensperger, U.: Aging of biogenic secondary organic aerosol via gas-phase OH radical reactions, P. Natl. Acad. Sci. USA, 109, 13503–13508, https://doi.org/10.1073/pnas.1115186109, 2012.

Emery, C. A., Tai, E., and Yarwood, G.: Enhanced meteorological modeling and performance evaluation for two Texas ozone episodes, Project Report prepared for the Texas Natural Resource Conservation Commissions, ENVIRON International Corporation, Novato, CA, 2001.

Fast, J. D., Gustafson, W. I., Easter, R. C., Zaveri, R. A., Barnard, J. C., Chapman, E. G., Grell, G. A., and Peckham, S. E.: Evolution of ozone, particulates, and aerosol direct radiative forcing in the vicinity of Houston using a fully coupled meteorology-chemistry-aerosol model, J. Geophys. Res.-Atmos., 111, D21305, https://doi.org/10.1029/2005jd006721, 2006.

Forkel, R., Werhahn, J., Hansen, A. B., McKeen, S., Peckham, S., Grell, G., and Suppan, P.: Effect of aerosol-radiation feedback on regional air quality – A case study with WRF/Chem, Atmos. Environ., 53, 202–211, https://doi.org/10.1016/j.atmosenv.2011.10.009, 2012.

Forkel, R., Balzarini, A., Baro, R., Bianconi, R., Curci, G., Jimenez-Guerrero, P., Hirtl, M., Honzak, L., Lorenz, C., Im, U., Perez, J. L., Pirovano, G., San Jose, R., Tuccella, P., Werhahn, J., and Zabkar, R.: Analysis of the WRF-Chem contributions to AQMEII phase2 with respect to aerosol radiative feedbacks on meteorology and pollutant distributions, Atmos. Environ., 115, 630–645, https://doi.org/10.1016/j.atmosenv.2014.10.056, 2015.

Forster, P., Storelvmo, T., Armour, K., Collins, W., Dufresne, J.-L., Frame, D., Lunt, D. J., Mauritsen, T., Palmer, M. D., Watanabe, M., Wild, M., and Zhang, H.: The Earth's Energy Budget, Climate Feedbacks, and Climate Sensitivity. In Climate Change 2021: The Physical Science Basis. Contribution of Working Group I to the Sixth Assessment Report of the Intergovernmental Panel on Climate Change, edited by: Masson-Delmotte, V., Zhai, P., Pirani, A., Connors, S. L., Péan, C., Berger, S., Caud, N., Chen, Y., Goldfarb, L., Gomis, M. I., Huang, M., Leitzell, K., Lonnoy, E., Matthews, J. B. R., Maycock, T. K., Waterfield, T., Yelekçi, O., Yu, R., and Zhou, B., Cambridge, United Kingdom and New York, NY, USA, Cambridge University Press, 923–1054, https://www.ipcc.ch/report/ar6/wg1/chapter/chapter-7/ (last access: 12 November 2023), 2021.

Gao, M., Han, Z., Tao, Z., Li, J., Kang, J.-E., Huang, K., Dong, X., Zhuang, B., Li, S., Ge, B., Wu, Q., Lee, H.-J., Kim, C.-H., Fu, J. S., Wang, T., Chin, M., Li, M., Woo, J.-H., Zhang, Q., Cheng, Y., Wang, Z., and Carmichael, G. R.: Air quality and climate change, Topic 3 of the Model Inter-Comparison Study for Asia Phase III (MICS-Asia III) – Part 2: aerosol radiative effects and aerosol feedbacks, Atmos. Chem. Phys., 20, 1147–1161, https://doi.org/10.5194/acp-20-1147-2020, 2020.

Gong, W., Makar, P. A., Zhang, J., Milbrandt, J., Gravel, S., Hayden, K. L., Macdonald, A. M., and Leaitch, W. R.: Modelling aerosol-cloud-meteorology interaction: A case study with a fully coupled air quality model (GEM-MACH), Atmos. Environ., 115, 695–715, https://doi.org/10.1016/j.atmosenv.2015.05.062, 2015.

Grell, G. A. and Freitas, S. R.: A scale and aerosol aware stochastic convective parameterization for weather and air quality modeling, Atmos. Chem. Phys., 14, 5233–5250, https://doi.org/10.5194/acp-14-5233-2014, 2014.

Guenther, A., Karl, T., Harley, P., Wiedinmyer, C., Palmer, P. I., and Geron, C.: Estimates of global terrestrial isoprene emissions using MEGAN (Model of Emissions of Gases and Aerosols from Nature), Atmos. Chem. Phys., 6, 3181–3210, https://doi.org/10.5194/acp-6-3181-2006, 2006.

Gustafson, W. I., Chapman, E. G., Ghan, S. J., Easter, R. C., and Fast, J. D.: Impact on modeled cloud characteristics due to simplified treatment of uniform cloud condensation nuclei during NEAQS 2004, Geophys. Res. Lett., 34, L19809, https://doi.org/10.1029/2007gl030021, 2007.

Iacono, M. J., Delamere, J. S., Mlawer, E. J., Shephard, M. W., Clough, S. A., and Collins, W. D.: Radiative forcing by long-lived greenhouse gases: Calculations with the AER radiative transfer models, J. Geophys. Res.-Atmos., 113, D13103, https://doi.org/10.1029/2008jd009944, 2008.

Janjic, Z. I.: The Step-Mountain Eta Coordinate Model – Further Developments Of the Convection, Viscous Sublayer, And Turbulence Closure Schemes, Mon. Weather Rev., 122, 927–945, https://doi.org/10.1175/1520-0493(1994)122<0927:Tsmecm>2.0.Co;2, 1994.

Kanji, Z. A., Ladino, L. A., Wex, H., Boose, Y., BurkertKohn, M., Cziczo, D. J., and Krämer, M.: Chapter 1: overview of ice nucleating particles, Meteor. Mon., 58, 1.1–1.33, https://doi.org/10.1175/amsmonographs-d-16-0006.1, 2017.

Kong, X., Forkel, R., Sokhi, R. S., Suppan, P., Baklanov, A., Gauss, M., Brunner, D., Baro, R., Balzarini, A., Chemel, C., Curci, G., Jimenez-Guerrero, P., Hirtl, M., Honzak, L., Im, U., Perez, J. L., Pirovano, G., San Jose, R., Schlunzen, K. H., Tsegas, G., Tuccella, P., Werhahn, J., Zabkar, R., and Galmarini, S.: Analysis of meteorology-chemistry interac-

tions during air pollution episodes using online coupled models within AQMEII phase-2, Atmos. Environ., 115, 527–540, https://doi.org/10.1016/j.atmosenv.2014.09.020, 2015.

Le, T., Wang, Y., Liu, L., Yang, J., Yung, Y. L., Li, G., and Seinfeld, J. H.: Unexpected air pollution with marked emission reductions during the COVID-19 outbreak in China, Science, 369, 702–706, https://doi.org/10.1126/science.abb7431, 2020.

Li, L., An, J. Y., Zhou, M., Yan, R. S., Huang, C., Lu, Q., Lin, L., Wang, Y. J., Tao, S. K., Qiao, L. P., Zhu, S. H., and Chen, C. H.: Source apportionment of fine particles and its chemical components over the Yangtze River Delta, China during a heavy haze pollution episode, Atmos. Environ., 123, 415–429, https://doi.org/10.1016/j.atmosenv.2015.06.051, 2015.

Li, S., Wang, S., Wu, Q., Zhang, Y., Ouyang, D., Zheng, H., Han, L., Qiu, X., Wen, Y., Liu, M., Jiang, Y., Yin, D., Liu, K., Zhao, B., Zhang, S., Wu, Y., and Hao, J.: Emission trends of air pollutants and CO_2 in China from 2005 to 2021, Earth Syst. Sci. Data, 15, 2279–2294, https://doi.org/10.5194/essd-15-2279-2023, 2023.

Lin, C. J.: Characteristics and Sources of Water-soluble Inorganic Ions in Atmospheric Particulate Matter and Rainfall in the suburb of Mianyang, Master, Southwest University of Science and Technology, https://doi.org/10.27415/d.cnki.gxngc.2022.000923, 2022.

Liu, Q., Jia, X. C., Quan, J. N., Li, J. Y., Li, X., Wu, Y. X., Chen, D., Wang, Z. F., and Liu, Y. G.: New positive feedback mechanism between boundary layer meteorology and secondary aerosol formation during severe haze events, Sci. Rep.-UK, 8, 6095, https://doi.org/10.1038/S41598-018-24366-3, 2018.

Liu, Y. Y., Xing, J., Wang, S. X., Fu, X., and Zheng, H. T.: Source-specific speciation profiles of $PM_{2.5}$ for heavy metals and their anthropogenic emissions in China, Environ. Pollut., 239, 544–553, https://doi.org/10.1016/j.envpol.2018.04.047, 2018.

Matthias, V., Aulinger, A., Bieser, J., Chen, Y. J., Geyer, B., Gao, J., Quante, M., and Zhang, F.: Modeling high aerosol loads in China in January 2013, Urban Clim., 22, 35–50, https://doi.org/10.1016/j.uclim.2016.04.005, 2017.

Moch, J. M., Mickley, L. J., Keller, C. A., Bian, H. S., Lundgren, E. W., Zhai, S. X., and Jacob, D. J.: Aerosol-Radiation Interactions in China in Winter: Competing Effects of Reduced Shortwave Radiation and Cloud-Snowfall-Albedo Feedbacks Under Rapidly Changing Emissions, J. Geophys. Res.-Atmos., 127, e2021JD035442, https://doi.org/10.1029/2021JD035442, 2022.

Morrison, H., Thompson, G., and Tatarskii, V.: Impact of Cloud Microphysics on the Development of Trailing Stratiform Precipitation in a Simulated Squall Line: Comparison of One- and Two-Moment Schemes, Mon. Weather Rev., 137, 991–1007, https://doi.org/10.1175/2008MWR2556.1, 2009.

Myhre, G., Stordal, F., Johnsrud, M., Kaufman, Y. J., Rosenfeld, D., Storelvmo, T., Kristjansson, J. E., Berntsen, T. K., Myhre, A., and Isaksen, I. S. A.: Aerosol-cloud interaction inferred from MODIS satellite data and global aerosol models, Atmos. Chem. Phys., 7, 3081–3101, https://doi.org/10.5194/acp-7-3081-2007, 2007.

Niu, G. Y., Yang, Z. L., Mitchell, K. E., Chen, F., Ek, M. B., Barlage, M., Kumar, A., Manning, K., Niyogi, D., Rosero, E., Tewari, M., and Xia, Y. L.: The community Noah land surface model with multiparameterization options (Noah-MP): 1. Model description and evaluation with local-scale measurements, J. Geophys. Res.-Atmos., 116, D12109, https://doi.org/10.1029/2010jd015139, 2011.

Rosenfeld, D., Sherwood, S., Wood, R., and Donner, L.: Climate Effects of Aerosol-Cloud Interactions, Science, 343, 379–380, https://doi.org/10.1126/science.1247490, 2014.

Savane, O. S., Vant-Hull, B., Mahani, S., and Khanbilvardi, R.: Effects of Aerosol on Cloud Liquid Water Path: Statistical Method a Potential Source for Divergence in Past Observation Based Correlative Studies, Atmosphere-Basel, 6, 273–298, https://doi.org/10.3390/atmos6030273, 2015.

Seinfeld, J. H., Bretherton, C., Carslaw, K. S., Coe, H., DeMott, P. J., Dunlea, E. J., Feingold, G., Ghan, S., Guenther, A. B., Kahn, R., Kraucunas, I., Kreidenweis, S. M., Molina, M. J., Nenes, A., Penner, J. E., Prather, K. A., Ramanathan, V., Ramaswamy, V., Rasch, P. J., Ravishankara, A. R., Rosenfeld, D., Stephens, G., and Wood, R.: Improving our fundamental understanding of the role of aerosol-cloud interactions in the climate system, P. Natl. Acad. Sci. USA, 113, 5781–5790, https://doi.org/10.1073/pnas.1514043113, 2016.

Shrivastava, M., Fast, J., Easter, R., Gustafson Jr., W. I., Zaveri, R. A., Jimenez, J. L., Saide, P., and Hodzic, A.: Modeling organic aerosols in a megacity: comparison of simple and complex representations of the volatility basis set approach, Atmos. Chem. Phys., 11, 6639–6662, https://doi.org/10.5194/acp-11-6639-2011, 2011.

Wang, H., Shi, G. Y., Zhang, X. Y., Gong, S. L., Tan, S. C., Chen, B., Che, H. Z., and Li, T.: Mesoscale modelling study of the interactions between aerosols and PBL meteorology during a haze episode in China Jing–Jin–Ji and its near surrounding region – Part 2: Aerosols' radiative feedback effects, Atmos. Chem. Phys., 15, 3277–3287, https://doi.org/10.5194/acp-15-3277-2015, 2015.

Wang, J. D., Wang, S. X., Jiang, J. K., Ding, A. J., Zheng, M., Zhao, B., Wong, D. C., Zhou, W., Zheng, G. J., Wang, L., Pleim, J. E., and Hao, J. M.: Impact of aerosol-meteorology interactions on fine particle pollution during China's severe haze episode in January 2013, Environ. Res. Lett., 9, 094002, https://doi.org/10.1088/1748-9326/9/9/094002, 2014.

Wang, J. D., Zhao, B., Wang, S. X., Yang, F. M., Xing, J., Morawska, L., Ding, A. J., Kulmala, M., Kerminen, V. M., Kujansuu, J., Wang, Z. F., Ding, D. A., Zhang, X. Y., Wang, H. B., Tian, M., Petaja, T., Jiang, J. K., and Hao, J. M.: Particulate matter pollution over China and the effects of control policies, Sci. Total Environ., 584, 426–447, https://doi.org/10.1016/j.scitotenv.2017.01.027, 2017.

Wang, L. W., Wen, L., Xu, C. H., Chen, J. M., Wang, X. F., Yang, L. X., Wang, W. X., Yang, X., Sui, X., Yao, L., and Zhang, Q. Z.: HONO and its potential source particulate nitrite at an urban site in North China during the cold season, Sci. Total Environ., 538, 93–101, https://doi.org/10.1016/j.scitotenv.2015.08.032, 2015.

Wang, Y. S., Li, W. J., Gao, W. K., Liu, Z. R., Tian, S. L., Shen, R. R., Ji, D. S., Wang, S., Wang, L. L., Tang, G. Q., Song, T., Cheng, M. T., Wang, G. H., Gong, Z. Y., Hao, J. M., and Zhang, Y. H.: Trends in particulate matter and its chemical compositions in China from 2013–2017, Sci. China Earth Sci., 62, 1857–1871, https://doi.org/10.1007/s11430-018-9373-1, 2019.

Wang, Z. F., Li, J., Wang, Z., Yang, W., Tang, X., Ge, B., Yan, P., Zhu, L., Chen, X., and Chen, H.: Modeling study of regional severe hazes over mid-eastern China in January 2013 and its implications on pollution prevention and control, Sci. China

Earth Sci., 57, 3–13, https://doi.org/10.1007/s11430-013-4793-0, 2014.

Wild, O., Zhu, X., and Prather, M. J.: Fast-j: Accurate simulation of in- and below-cloud photolysis in tropospheric chemical models, J. Atmos. Chem., 37, 245–282, https://doi.org/10.1023/A:1006415919030, 2000.

Wu, J. R., Bei, N. F., Hu, B., Liu, S. X., Wang, Y., Shen, Z. X., Li, X., Liu, L., Wang, R. N., Liu, Z. R., Cao, J. J., Tie, X. X., Molina, L. T., and Li, G. H.: Aerosol-photolysis interaction reduces particulate matter during wintertime haze events, P. Natl. Acad. Sci. USA, 117, 9755–9761, https://doi.org/10.1073/pnas.1916775117, 2020.

Xiong, C. R., Li, J., Liu, Z. X., and Zhang, Z. Y.: The dominant role of aerosol-cloud interactions in aerosol-boundary layer feedback: Case studies in three megacities in China, Front. Env. Sci.-Switz, 10, 1002412, https://doi.org/10.3389/Fenvs.2022.1002412, 2022.

Xue, C. Y., Zhang, C. L., Ye, C., Liu, P. F., Catoire, V., Krysztofiak, G., Chen, H., Ren, Y. G., Zhao, X. X., Wang, J. H., Zhang, F., Zhang, C. X., Zhang, J. W., An, J. L., Wang, T., Chen, J. M., Kleffmann, J., Mellouki, A., and Mu, Y. J.: HONO Budget and Its Role in Nitrate Formation in the Rural North China Plain, Environ. Sci. Technol., 54, 11048–11057, https://doi.org/10.1021/acs.est.0c01832, 2020.

Zaveri, R. A., Easter, R. C., Fast, J. D., and Peters, L. K.: Model for Simulating Aerosol Interactions and Chemistry (MOSAIC), J. Geophys. Res.-Atmos., 113, D13204, https://doi.org/10.1029/2007jd008782, 2008.

Zhang, B., Wang, Y., and Hao, J.: Simulating aerosol–radiation–cloud feedbacks on meteorology and air quality over eastern China under severe haze conditionsin winter, Atmos. Chem. Phys., 15, 2387–2404, https://doi.org/10.5194/acp-15-2387-2015, 2015.

Zhang, F. F.: Characteristics of Air Pollution and Chemical Composition of $PM_{2.5}$ in Handan Master, College of Urban Construction, Hebei University of Engineering, https://www.cnki.net/KCMS/detail/detail.aspx?dbcode=CMFD&dbname=CMFD201601&filename=1015375754.nh&uniplatform=OVERSEA&v=2wa2h1BY1IjK8oKoBzUjfC3NyHI9ey1UGVZYwOQ2-Q4PP76c8MmlzWxRmVRvrv7 (last access: 12 November 2023), 2015.

Zhang, F., Wang, Y., Peng, J. F., Chen, L., Sun, Y. L., Duan, L., Ge, X. L., Li, Y. X., Zhao, J. Y., Liu, C., Zhang, X. C., Zhang, G., Pan, Y. P., Wang, Y. S., Zhang, A. L., Ji, Y. M., Wang, G. H., Hu, M., Molina, M. J., and Zhang, R. Y.: An unexpected catalyst dominates formation and radiative forcing of regional haze, P. Natl. Acad. Sci. USA, 117, 3960–3966, https://doi.org/10.1073/pnas.1919343117, 2020.

Zhang, F. F., Xing, J., Ding, D. A., Wang, J. D., Zheng, H. T., Zhao, B., Qi, L., and Wang, S. X.: Role of black carbon in modulating aerosol direct effects driven by air pollution controls during 2013–2017 in China, Sci. Total Environ., 832, 154928, https://doi.org/10.1016/j.scitotenv.2022.154928, 2022.

Zhang, X., Zhang, Q., Hong, C. P., Zheng, Y. X., Geng, G. N., Tong, D., Zhang, Y. X., and Zhang, X. Y.: Enhancement of $PM_{2.5}$ Concentrations by Aerosol-Meteorology Interactions Over China, J. Geophys. Res.-Atmos., 123, 1179–1194, https://doi.org/10.1002/2017JD027524, 2018.

Zhao, B., Liou, K. N., Gu, Y., Li, Q. B., Jiang, J. H., Su, H., He, C. L., Tseng, H. L. R., Wang, S. X., Liu, R., Qi, L., Lee, W. L., and Hao, J. M.: Enhanced $PM_{2.5}$ pollution in China due to aerosol-cloud interactions, Sci. Rep.-UK, 7, 4453, https://doi.org/10.1038/S41598-017-04096-8, 2017.

Zhao, C., Liu, X., Leung, L. R., Johnson, B., McFarlane, S. A., Gustafson Jr., W. I., Fast, J. D., and Easter, R.: The spatial distribution of mineral dust and its shortwave radiative forcing over North Africa: modeling sensitivities to dust emissions and aerosol size treatments, Atmos. Chem. Phys., 10, 8821–8838, https://doi.org/10.5194/acp-10-8821-2010, 2010.

Zhao, C., Chen, S., Leung, L. R., Qian, Y., Kok, J. F., Zaveri, R. A., and Huang, J.: Uncertainty in modeling dust mass balance and radiative forcing from size parameterization, Atmos. Chem. Phys., 13, 10733–10753, https://doi.org/10.5194/acp-13-10733-2013, 2013.

Zheng, H., Cai, S., Wang, S., Zhao, B., Chang, X., and Hao, J.: Development of a unit-based industrial emission inventory in the Beijing–Tianjin–Hebei region and resulting improvement in air quality modeling, Atmos. Chem. Phys., 19, 3447–3462, https://doi.org/10.5194/acp-19-3447-2019, 2019.

Zhou, M., Zhang, L., Chen, D., Gu, Y., Fu, T. M., Gao, M., Zhao, Y. H., Lu, X., and Zhao, B.: The impact of aerosol-radiation interactions on the effectiveness of emission control measures, Environ. Res. Lett., 14, 024002, https://doi.org/10.1088/1748-9326/Aaf27d, 2019.